Observing Crab Pulsar Properties with JBO's 42ft Radio Telescope
Third Year Lab Report

Jade Salisbury
Department of Physics and Astronomy, University of Manchester
(Experiment performed in collaboration with S. Novak)
(Dated: March 05, 2024)

The Crab Pulsar is a supernova remnant in the Crab Nebula. Using the 42ft radio telescope at Jodrell Bank Observatory, the spin period (P) and spin-down rate ($\dot{P}$) were calculated to be $0.03339375 \pm 0.00000008$s and $(4.184 \pm 0.002) \times 10^{-13}$ respectively by using multi-variable least-squares fitting algorithms with data from 6 observations over 8 weeks (February to April, 2024). From these values, the characteristic age (1270 ± 10yrs) and surface magnetic field strength ($(3.78 \pm 0.01) \times 10^{12}$ gauss) were calculated. The main source of error on these values is as a result of template matching to find arrival times and weighted least squares fitting.

1. INTRODUCTION

At the end of a main-sequence star's lifetime, higher mass stars of around $8 - 15\mathrm{M}_\odot$ solar masses can end in violent explosions known as (type II/core collapse) supernovae after the core of the star implodes under its own gravity. The inner layers of the star collapse into the core and the outer layers bounce back outwards, leaving a supernova remnant in the surrounding area of space. The resulting free core is known as a neutron star. Neutron stars have a typical mass of around $1.4\mathrm{M}_\odot$ [1] and a neutron star with a mass greater than $2.2 - 2.9\mathrm{M}_\odot$ will continue to collapse into a singularity known as a black hole [2]. The Crab Pulsar is one such neutron star and the Crab Nebula is its supernova remnant.

Pulsars are highly magnetised, quickly spinning neutron stars that rotate as a result of conservation of momentum from their formation in a supernova; most pulsars have rotation periods between 0.25 and 1 seconds [3]. They are characterised by a lighthouse-like beam of electromagnetic radiation which sweeps across the sky with their rotations, appearing as regular pulsing from Earth. The periodic pulses can be detected with radio telescopes such as the 42ft dish at Jodrel Bank Observatory.

Measuring the characteristics of a pulsar is involved, but provides a lot of information about attributes such as the structure of neutron stars, their magnetic field strength and age. This experiment focuses on finding the latter two through measurement and algorithmic fitting of the pulsar spin period, P, and the rate of increase in period, or spin-down, $\dot{P}$.

2. THEORY

2.1. *Dispersion*

As the pulsed radiation from the pulsar travels through the interstellar medium (ISM) it becomes dispersed. The ionised gas causes light to travel at speed v_g,

$$v_g = c\left[1 - \frac{n_e r_o \lambda^2}{2\pi}\right], \tag{1}$$

where c is the speed of light, n_e is the electron density in the ISM, $r_o = e^2/m_e c^2$ [1] (classical electron radius) and λ the wavelength [3]. The wavelength dependence in Equation 1 results in reduced velocity and therefore altered pulse arrival for every frequency. This is known as dispersion, and to counteract it an appropriate, frequency dependant delay must be added.

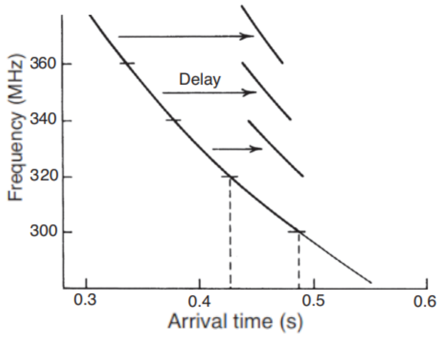

FIG. 1. The process of de-dispersion, achieved by adding a frequency dependent delay to each frequency channel. Image altered from [3].

The amount that light is dispersed along the line of sight is represented by the dispersion measure, DM $= \int_0^L n_e \mathrm{d}l$ where L is the distance to the pulsar, often measured in pccm^{-3}. Using Equation 1 and the definition of DM, the delay added at a given frequency bin to counteract dispersion is

$$t = 4.15 \times 10^3 \text{ DM } \nu_{\mathrm{MHz}}^{-2} \text{ s}, \tag{2}$$

where ν_{MHz} is the frequency in MHz [3], the result of this 'de-dispersion' is demonstrated in Figure 1. If the DM is known accurately for a pulsar, its distance estimated through an assumption of a roughly constant $n_e \approx 0.033\mathrm{cm}^{-3}$ [4] along the line of sight.

2.2. *Derived parameters*

Particle outflow (wind), magnetic dipole radiation and gravitational radiation are the origins of pulsar kinetic energy loss and therefore spin-down [5]. In classical electrodynamics, the rate at which a spinning magnetic dipole radiates a wave at frequency Ω with power is,

$$\frac{\mathrm{d}(\frac{1}{2}I\Omega^2)}{\mathrm{d}t} = I\Omega\dot{\Omega} = \frac{2}{3}M_\perp^2\Omega^4c^{-3}, \tag{3}$$

and is equal to the rate of change of kinetic energy under the assumption that minimal energy is lost

[1] e and m_e are the electron charge and mass respectively; c is the speed of light.

through other means, though the total energy flow can still be approximated with Equation 3, even if the inverse is true [3]. Measured values of P and $\dot{P}$ can derive the magnetic moment M which can then be used to find the approximate value of the surface magnetic field at the poles, B_0 with

$$B_0 = 3.3 \times 10^{19} (P\dot{P})^{\frac{1}{2}} \text{ gauss.} \quad (4)$$

If it is assumed that the pulsar is formed with a high initial angular velocity and evolved in accordance with a simple power law, it can be retrieved that $\dot{\Omega} = -k\Omega^n$, where Ω and $\dot{\Omega}$ are the angular velocity and rate of change of angular velocity. n is referred to as the 'breaking index' [3]. From this it can be derived that the approximate age of a pulsar is equal to

$$\tau = -\frac{1}{n-1}\frac{\Omega}{\dot{\Omega}} = \frac{1}{n-1}\frac{P}{\dot{P}}. \quad (5)$$

For only magnetic dipole breaking, $n = 3$ and then $\tau = \frac{1}{2}P\dot{P}$ and defines the the the 'characteristic age'. Differing values of n suggest substantial energy loss through particle wind or gravitational radiation [5].
Interesting properties can be found through finding an accurate value for the rate of change of spin-down, $\ddot{P}$. Most notably the breaking index is derived in [3] as

$$n = 2 - \frac{P\ddot{P}}{\dot{P}^2} \quad (6)$$

To find any value of $\ddot{P}$, periods of observations must be over years or decades. Therefore, $\ddot{P}$ will not be fit for in this experiment and an assumption must be made ($n = 3$) or data from other experiments must be used ($n \approx 2.5$ from [3]).

3. METHODOLOGY

3.1. *Generating TOAs*

Observations made by the 42ft telescope can have any integration time. A single observation will be made up of many sub-integrations of ~ 200 seconds, each folded onto themselves with an approximate period to improve the signal/noise ratio (S/N). For each sub-integration, the telescope takes measurements of the incoming radiation between frequencies 606 and 616MHz into 40 'bins' or 'channels' of width 250kHz. To reduce data volume and increase S/N, incoming signal is integrated over time by summing the power received for each channel over a sub-integration.
A simple fitting algorithm for finding the DM to the pulsar was used by finding each integrated profile[2] peak for every DM from 0 to 200 in intervals of 0.1 (pccm^{-3}), then selecting the DM through quadratic fitting from the set of DMs with the highest peaks.
The data was then de-dispersed and frequency-averaged. A Fourier Phase Gradient Scheme (PGS), which is a 'template matching' method detailed in [6] was used; through PSRCHIVE [7], a single TOA was generated for each sub-integration, corresponding to the arrival time of a single pulse within it.

[2] The integrated profile refers to a number proportional to the full added signal over each frequency band.

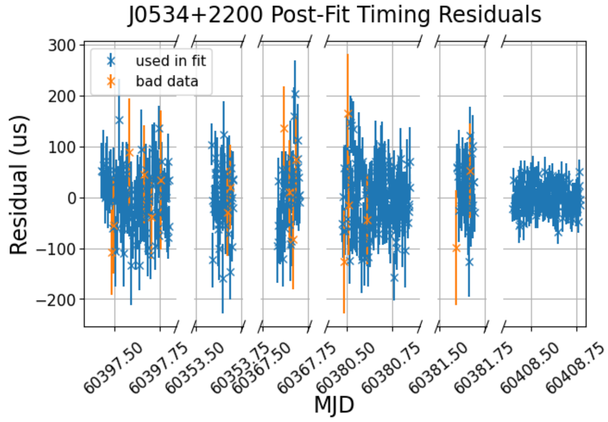

FIG. 2. Residuals for all 6 observations over the course of 8 weeks on a broken x-axis. Each 'block' is 2 weeks apart, except blocks 3 and 4 which are only one day apart. TOAs with an error $\geq$ 80μs were considered 'bad' and were not included in fitting.

3.2. *Corrections to TOAs*

In order to accurately time the pulsar, each pulse arrival time needs to be recorded as if it arrived at the same location, regardless of where it was measured. The location picked is the barycentre of the solar system. Correcting for pulse time arrivals due to the location of the Earth in its orbit around the sun requires an ephemeris[3][8]. To account for the difference, the TOAs must be adjusted by the amount of time taken for light to travel to the barycentre from the Earth's centre (Römer delay), and then again with the time light would take to travel from the observatory to the centre of Earth (Earth delay). In additional to dynamical delays, there are some smaller, relativistic effects that must also be adjusted for: Einstein delay accounts for the time dilation as a result of the pulsar moving and Shapiro delay accounts for the general relativistic effect from the curve of spacetime around the Sun and the pulsar.

3.3. *PINT*

For fitting the TOAs to various parameters there are several popular software packages, the most popular being Tempo2 [9]. For ease of use and familiarity with Python, PINT [10] was chosen for this experiment. Both packages achieve similar results but were developed independently, at different times and are known to agree with each other up to ~10 nanoseconds[4].
Following the PINT documentation, the value of P, can be found accurately in relatively short observations of several hours through weighted least squares fitting (WLS). It is more challenging to find $\dot{P}$ and often requires some weeks of observation. Sometimes PINT would incorrectly guess the pulse number (PN) of whole groups of TOAs, and they would have to be changed manually by increasing or decreasing their PN by 1 or 2 so that a sensible fit could be found.

[3] https://en.wikipedia.org/wiki/Ephemeris
[4] https://github.com/nanograv/PINT

Property	Value	Units
P	$0.03339375 \pm 0.00000008$	seconds
$\dot{P}$	$(4.184 \pm 0.002) \times 10^{-13}$	unitless
B_0	$(3.78 \pm 0.01) \times 10^{12}$	gauss
τ	1270 ± 10	years

TABLE I. A table showing fitted parameters: period, P, and spin-down rate, $\dot{P}$; and derived parameters: surface magnetic field strength, B_0, and characteristic age, τ.

4. RESULTS

4.1. Dispersion measure and distance

Using the method in Section, 3.1, a DM of 57 ± 5pccm^{-3} was found, corresponding to a distance of 1900 ± 200pc. The de-dispersion algorithm was set up with a DM of 57 using Equation 2, and moderately removed the effect of dispersion. For the remainder of the experiment the accepted value of 56.77 [11] was used due to the large error on the value obtained by polynomial fitting. With an accurate DM, the data was de-dispersed and TOAs were found, corrected, and put through PINT for fitting.

4.2. Crab Pulsar properties

To fit the data for P, the (corrected) TOAs from the two observations closest in time were fitted to a constant P using a WLS algorithm. As these two observations were only one day apart, the period was roughly constant and could be found in this range. With a more accurate P, the additional data from the 4 observations in the 8 weeks surrounding the 2 consecutive observations were added to the fit, which was expanded to also fit for $\dot{P}$, giving the values in Table I. From these values and the equations in Section 2, values for B_0 and τ could be found. The largest source of error is from the PGS algorithm, though they are still underestimated [12]. The final post-fit timing residuals are shown in Figure 2 and the best fit has $\chi^2_R = 1.29$.

5. DISCUSSION

Fitting with just two variables, P and $\dot{P}$, allows the parameters to give residual spread shown in Figure 2, with residuals of order ±100µs. One reason for non-zero residuals is due to the timing noise of the pulsar. All pulsars exhibit timing noise but it is most strong in younger pulsars and the Crab Pulsar is the youngest known pulsar [3].
The reduced residual spread in the final observation suggests that the fit is more accurate for the TOAs therein. One possible explanation is that it is possible to fit for a third time-varying parameter on an 8 week scale. However, as the χ^2_R of 1.29 shows, the spread of TOAs is statistically expected from the errors, therefore to improve the accuracy of the fit, the errors on must reduced/improved. The PGS method used to retrieve the TOAs and errors is known to underestimate the errors on TOAs for observations with low S/N [12], a notable property of the 200s sub-integrations in this experiment. To improve the quality of the errors a Gaussian interpolation (GIS) method could be used, as it is better suited for low S/N data, or the sub-integration time could be increased. Any additional observations will also improve the accuracy of P and $\dot{P}$.

6. CONCLUSIONS

The DM value of 57 ± 5pccm^{-3} is close to the known value of 56.77 from [11], though by chance due to the very large errors from the polynomial fitting algorithm used. The value obtained for P of $0.03339375 \pm 0.00000008$s is remarkably close to the accepted (current day) value of 0.03339241s from [11]. Similarly, the value retrieved for $\dot{P}$ is $(4.184 \pm 0.002) \times 10^{-13}$ and the [11] value is 4.209×10^{-13}. Despite the closeness, it is very clear that the errors derived are underestimates as they do not contain the accepted values. It can be assumed that B_0 (1270 ± 10yrs) and τ ($(3.78 \pm 0.01) \times 10^{12}$ gauss) are accurate within each of their respective equation limitations due to the apparent closeness of the fitted parameters. The supernova forming the Crab Pulsar was documented in 1054AD [3]. Therefore it a known age of 970 years, differing from the characteristic age and further proving that the pulsar does not act as a perfect magnetic dipole.

[1] M. Seeds and D. Backman, *Astronomy: The Solar System and Beyond* (Cengage Learning, 2009).
[2] V. Kalogera and G. Baym, The Astrophysical Journal **470**, L61–L64 (1996).
[3] A. G. Lyne and F. Graham-Smith, *Pulsar astronomy*, Cambridge astrophysics series ; 16 (Cambridge University Press, Cambridge, 1990).
[4] J. G. Ables and R. N. Manchester, aap **50**, 177 (1976).
[5] O. Hamil, Braking index of isolated pulsars: open questions and ways forward (2015), arXiv:1503.09110 [astro-ph.HE].
[6] J. H. Taylor, Philosophical Transactions: Physical Sciences and Engineering **341**, 117 (1992).
[7] W. van Straten, P. Demorest, and S. Osłowski, Pulsar data analysis with psrchive (2012), arXiv:1205.6276 [astro-ph.IM].
[8] W. M. Folkner, J. G. Williams, and D. H. Boggs, Interplanetary Network Progress Report **42-178**, 1 (2009).
[9] G. B. Hobbs, R. T. Edwards, and R. N. Manchester, Monthly Notices of the Royal Astronomical Society **369**, 655–672 (2006).
[10] J. Luo, S. Ransom, P. Demorest, P. S. Ray, A. Archibald, M. Kerr, R. J. Jennings, M. Bachetti, R. van Haasteren, C. A. Champagne, J. Colen, C. Phillips, J. Zimmerman, K. Stovall, M. T. Lam, and F. A. Jenet, The Astrophysical Journal **911**, 45 (2021).
[11] R. N. Manchester, G. B. Hobbs, A. Teoh, and M. Hobbs, The Astronomical Journal **129**, 1993–2006 (2005).
[12] Wang, J., Shaifullah, G. M., Verbiest, J. P. W., Tiburzi, C., Champion, D. J., Cognard, I., Gaikwad, M., Graikou, E., Guillemot, L., Hu, H., Karuppusamy, R., Keith, M. J., Kramer, M., Liu, Y., Lyne, A. G., Mickaliger, M. B., Stappers, B. W., and Theureau, G., A&A **658**, A181 (2022).